Polarimetric Cloud Analysis and Seeding Test (POLCAST)

Paul A. Kucera[1,2], Adam Theisen[1], and Darin Langerud[3]

[1]Department of Atmospheric Sciences, University of North Dakota, Grand Forks, North Dakota, USA
[2]Research Applications Laboratory, National Center for Atmospheric Research, Boulder, Colorado, USA
[3]North Dakota Atmospheric Resource Board, Bismarck, North Dakota, USA

ABSTRACT

The Polarimetric Cloud Analysis and Seeding Test (POLCAST) was a cloud seeding research experiment that was conducted to help determine if hygroscopic seeding could be detected directly by polarimetric radar observations or through derived polarimetric parameters. The operational phase of the program, a cooperative study between the North Dakota Atmospheric Resource Board (NDARB), University of North Dakota, Weather Modification Inc., and Ice Crystal Engineering, was conducted from 10 July – 5 August 2006. The study was centered on the measurements recorded by the University of North (UND) C-Band polarimetric Doppler Radar (NorthPol). Hygroscopic flares, deployed on a Weather Modification Incorporation (WMI) aircraft, were used in the study. Ice Crystal Engineering provided these flares.

From the polarimetric radar observations, liquid water content, rainfall rates and hydrometeor type were analyzed. The radar-estimated liquid water content retrievals indicated an increase in 7 of the 8 cases after hygroscopic seeding. In correspondence, the rainfall rates were also higher along with the durations of the cells in the seeded cases. The differential reflectivity decreased after seeding, which is an indication that rain drops were decreasing on average in size. The reflectivity also increased after seeding except at cloud base where there was a decrease in reflectivity after seeding. The hydrometeor identification results were in good agreement with the trends observed in reflectivity and differential reflectivity fields.

1. Introduction

The Polarimetric Cloud Analysis and Seeding Test (POLCAST) was an experiment designed to help determine if hygroscopic seeding could be detected by polarimetric radar observables or by derived radar fields. The operational phase of the program, a cooperative study between the North Dakota Atmospheric Resource Board (NDARB), University of North Dakota (UND), Weather Modification Inc., and Ice Crystal Engineering, was conducted from 10 July to 5 August 2006. Ice Crystal Engineering provided the flares used during the project. Weather Modification Inc. operated the seeding aircraft while the UND C-Band Polarimetric Doppler Radar (NorthPol) observed the clouds that were seeded (and unseeded). NorthPol collected a variety of radar observables, which included radar reflectivity, Doppler velocity, differential reflectivity, differential phase, specific differential phase, and the correlation between the horizontal and vertical polarimetric fields (see Bringi and Chandrasekar (2001) and references therein for complete descriptions of polarimetric parameters). From the radar observations, liquid water content (LWC), rainfall rates, differential reflectivity and hydrometeor type were analyzed.

The experiment and data are discussed in section 2. The methodology for analysis is presented in section 3. The results are discussed in section 4. Section 5 presents the conclusions for our study.

2. Data Collection

Ideally, the radar operated each time a convective storm was within 100 km of the radar. Only a few potential cases were not examined during the experiment because of hardware problems or the lack of personnel to operate the radar. Scanning strategies included sector scans centered on the cells of interest or areas of new growth. Range Height Indicator (RHI) scans were used within the most intensive core of the storm and new growth regions. These scanning strategies provided high spatial and temporal resolution of the storm system to better understand the life-cycle characteristics. When not in high-resolution scanning mode, the radar was operated in full-volume Plan Position Indicator (PPI) mode. These scans have

Corresponding author address: Paul A. Kucera, NCAR/Research Applications Laboratory, P.O. Box 3000, Boulder, CO 80307, Ph: 303-386-3243; Fax: 303-386-8401, E-mail: pkucera@ucar.edu

a lower temporal resolution compared to sector scans but still provided useful information for the study.

During the summer of 2006, a total of eight cells were seeded during POLCAST. On days that convective storms were forecast, NorthPol scientists and the WMI pilot were put on standby. If the radar detected convective cells on a particular day, the seeding aircraft was directed to an area of isolated cells that had the potential for the development of new convection. After the seeding aircraft reached the target location, the pilot assessed the clouds in the area to determine if there were seeding candidates. Criteria the pilot looked for were a flat and solid rain-free cloud base, visual indications of cloud growth, cloud width of at least 1 km, and an updraft of at least 1 m s^{-1}. Updraft velocity was estimated by the use of power settings for level flight with vertical motion measured by the vertical speed indicator. Note that these subjective criteria could lead to bias in the results, and ideally, a randomized seeding experiment would be conducted. This was an exploratory study, however, and based on the results that follow, a confirmatory, randomized experiment would be a natural continuation of the initial work.

Ideally, the targeted cells had the following characteristics: a sustained updraft of 1-4 m s^{-1}, growth through the freezing level for supercooled water to be present, and were early enough in their development that precipitation was not observed below cloud base. Radar observations were used initially to determine a general location of a storm complex. However, most of the targeted cells observed by the pilot were either below or just at the minimum detectable level of the radar at selection time; but they were usually detectable within 5-10 min as the cell continued to develop. Once the cell was determined to be a candidate for the study, seeding was conducted just below cloud base in the rain-free updraft region of the cell by the aircraft. At the same time, NorthPol switched from full-volume mode to sector scans to capture the evolution of the targeted cell at a high spatial and temporal resolution until the cell either dissipated or it was out of range.

3. Methodology

A. Liquid Water Content Estimation

A variety of polarimetrically based algorithms were initially used to derive LWC from the radar observations. These derived fields were then compared to previously reported LWC from previous studies of convective clouds (Bringi et al 1992; Hu et al 1998; Hudak and List 1988). The algorithm that proved physically realistic and was consistent with the previous studies was implemented for the rest of the radar analyses. The equations for calculating the LWC polarimetric radar observations, W, in g m^{-3} are defined by the following algorithms:

Zh-ZDR

$$W(Z_H, ZDR) = 0.6*10^{-3}*Z_H^{(0.85)} *10^{(0.1*-2.36*ZDR)} , \quad (1)$$

where

$$Z_H = 10^{(dBZ/10)} \quad (2)$$

KDP

$$W(KDP) = 3.565*(KDP/5.6)^{0.77} , \quad (3)$$

where 5.6 is the frequency of the radar in GHz and KDP is in km^{-1}.

KDP-ZDR

$$W(KDP, ZDR) = 2.32*KDP^{0.83} * 10^{0.1*-1.11 * ZDR} \quad (4)$$

These algorithms are based on the material presented in Bringi and Chandrasekar (2001). It should be noted that the LWC in this context refers to the amount of liquid water detected by radar, which generally only observes precipitation-size hydrometeors (e.g., raindrops). Therefore, LWC used in this study is an underestimate of the total liquid water content (e.g., there is no contribution from cloud droplet size hydrometeors). However, the focus of the study was quantification of the relative change in contribution of precipitation to the LWC between seeded and unseeded cases, which the radar-derived LWC algorithms seemed to do quite well.

The average change of the LWC for all the seeded or unseeded cases relative to the maximum LWC (LWC_{MAX}) for each case above cloud base was standardized using the following relationship:

$$\frac{W_{t+1} - W_t}{LWC_{MAX}} , \quad (5)$$

where W_{t+1} is the LWC at time t+1 when compared relative to the LWC at time t (e.g., W_t). These values were then averaged for all of the cases at the recorded times after first cell detection. A standard deviation test was then applied to the data to remove any outliers. Outliers for our study were defined as those that were more than $\pm$ 2 standard deviations from the mean for the given height. The standard deviation test (± 2 STD) was applied in an effort to remove outliers

due to inherent noise in the radar data. This could remove important information at the upper and lower limits of radar-derived LWC. In the future, the implications of applying an outlier test will be examined but is beyond the scope of this study. This test assumed the transformed field had a normal distribution. If valid, then approximately 95% of the data were within 2 standard deviations. The data were also quality controlled using a moving average of length 5 to fit the data using a linear interpolation between the points. The results for LWC were then reported as fractional change relative to the maximum LWC observed. Note that ZDR and rainfall rates were also reported using the normalization in equation (5) (e.g., ZDR_{MAX} and $RainfallRate_{MAX}$ in the denominator).

B. ZDR

The differential reflectivity ZDR is defined as the logarithmic (times 10) value of the ratio of linear horizontal reflectivity compared to the linear vertical reflectivity. ZDR is dependent on the shape of the hydrometeors and can provide some indication of the size of the particles. For example, if observing raindrops, a value of ZDR around 0 dB would indicate the drops tend to be nearly spherical. If the ZDR is large (~3 dB), then the raindrops are likely to be spheroid shaped, which is an indication of larger raindrops. Kennedy et al. (2001) states that raindrops larger than 1.5 mm in diameter start to become oblate spheroids, where the backscattering cross-sectional area will be greater in the horizontal than in the vertical, producing a larger ZDR. Using the ZDR field with reflectivity can determine the presence of hail. Hail signature tends to have near-zero ZDR and high reflectivity values whereas regions with large raindrops tend to have high ZDR and reflectivity values (May and Keenan 2005).

C. Rainfall Rate Estimation

A study by Yan Yin et al. (2001) indicated that hygroscopic seeding should initiate rain earlier, produce more rain and extend the life of a seeded cloud. The rainfall rate was calculated using the Marshall and Palmer (1948) reflectivity – rainfall (Z-R) relationship of:

$$z = 200R^{1.6} \tag{6}$$

where z is the reflectivity in linear units of $mm^6\ m^{-3}$ and R is the rainfall rate in mm h^{-1}. Solving this equation for the rainfall rate R produces the equation:

$$R = \left[\frac{z}{200}\right]^{\frac{1}{1.6}} \tag{7}$$

Many different effects, such as hail contamination, beam blockage, attenuation and non-uniform beam filling, can affect the relationship (Austin 1987). According to Yan Yin et al. (2001), it is not realistic to expect the same Z-R relationship to work for both the seeded and unseeded cases. The conceptual model states that hygroscopic seeding widens the drop size distribution, leading to enhanced production of larger particles. However, the development of a unique Z-R for the region and for seeded and unseeded cells was outside the scope of this study. The goal of the study was to determine the relative changes between seeded and unseeded convective storms, and the absolute amount of rainfall was not critical but should be addressed in future evaluations.

D. Hydrometeor Identification

A hydrometeor identification program was based on the use of fuzzy-logic membership functions developed by Liu and Chandrasekar (2000). This algorithm was developed for S-band radars, which could have different base functions than NorthPol (C-band). However, studies by Straka et al. (2000) and May and Keenan (2005) indicate the membership functions have very similar values at S-Band and C-Band, respectively. A more significant issue at C-Band is likely differential attenuation between the horizontal and vertical reflectivity (Carey et al. 2000), especially through strong convective cores and long-paths of intervening rainfall. A correction can be applied at C-Band using the differential propagation phase (e.g., see Carey et al. 2000). This correction algorithm was not applied to the dataset. This will likely cause errors in the retrieval; however, we feel that the hydrometeor identification algorithm provides useful information on the relative distribution of hydrometeors in the study. The fuzzy logic algorithm categorizes the hydrometeors into 11 categories, which are defined in Table 1.

Table 1. Hydrometeor identification number and type as determined in the hydrometeor identification algorithm (Liu and Chandrasekar 2000).

Category Number	Hydrometeor Type
1	Drizzle
2	Rain
3	Dry Snow
4	Wet Snow
5	Vertical Ice
6	Dry Graupal
7	Wet Graupal
8	Small Hail
9	Large Hail
10	Small Hail and Rain
11	Large Hail and Rain

4. Results

A comparison of the different polarimetric LWC algorithms was performed for a subset of the cases. For all the comparisons, the *KDP* and *KDP-ZDR* LWC algorithms gave significantly higher estimates of LWC compared to the Z_h-*ZDR* algorithm. Also the LWC from the KDP-based algorithms was higher than what would be expected in the observed clouds. The Z_h-*ZDR* algorithm gave realistic estimates of LWC in comparison to previous studies (e.g., Bringi et al, 1997). Therefore, the Z_h-*ZDR* algorithm was used to estimate the LWC throughout the study. However, the Z_h-*ZDR* algorithm did produce LWC high values occasionally when ice was present, so the maximum LWC value was capped at 15 g m^{-3}. The Z_h-*ZDR* LWC on average did not exceed 4 g m^{-3}, however, and the number of high retrieved LWC values was small.

The radar data collected during POLCAST were used to look at the average differential reflectivity and liquid water content at 1 km $\pm$ 0.5 km intervals above cloud base to a maximum height of 12 km. Data were separated into levels above and below the freezing level. The seeding aircraft reported the cloud bases during the assessment of the cell. The reported cloud bases and the corresponding reported cloud base temperatures are given in Table 2. The cloud base temperatures were not reported by the pilot on two of the days. The sounding in Bismarck was used to estimate cloud base temperatures on these days. The temperature was taken as the environmental temperature corresponding to the cloud base height. The rainfall rate and hydrometeor identification were also analyzed using the radar data. The results from the seeded cases were then compared to unseeded cases in order to determine if there were any differences in characteristics between them. Unseeded cases selected for comparison had similar radar attributes to the seeded cases at the beginning of their lifecycle. Therefore, the seeded and unseeded cases had similar attributes before they were or would have been seeded. These attributes included cell size, duration, maximum intensity, and vertical structure. The unseeded cases were selected near the same time and location (but outside the target and downwind region of the seeded cell). This was done in an effort to sample the cases with the same environmental conditions (e.g., temperature, moisture, dynamics, and available cloud condensation nuclei). The main focus of analysis was to observe the effects of seeding in the core of the cell. For this study, the core of the cell was considered to be reflectivities greater than or equal to 30 dBZ.

Table 2. Cloud base heights and temperatures.

Date	1st Reported Cloud Base Height	2nd Reported Cloud Base Height	Cloud Base Temps
YYMMDD	m (ft)	m (ft)	°C
060711	2400 (8000)	2700 (9000)	10
060724	2100 (6800)	2400 (8000)	12
060725	900 (3000)	1500 (5000)	
060727	2500 (8200)		12
060804	3400 (11000)		
060805	2600 (8700)		10
060805	1100 (3700)		23

I. Liquid Water Content

The release of hygroscopic seeding material was focused around the updraft of the cell, since higher LWCs are normally near the updraft. The seeding material would then need less time to completely dissolute. Tzivion et al. (1994) found that the time for dry NaCl to dissolute is less than 1 s for particles of 5 μm. The flares used in the experiment were also of a salt compound, primarily potassium perchlorate and calcium chloride, which have been shown to produce particles of sizes 0.2 – 3.0 μm range (Roelof et al. 2005). It would be expected that these would also dissolute completely in a time of less than 1s after they are initially introduced. The conceptual model suggests seeding would create more raindrops that are detectable by radar relatively quickly, and based on the equations would show an increase in LWC. It should be noted that the discussion focuses on radar-derived liquid water content.

a. Unseeded Cases

The analysis of the unseeded cells did produce some consistent results with the LWC first reaching a maximum at higher levels and then the lower levels reaching a maximum at a later time such as the example shown in Fig. 1. A consistent pattern can be seen with LWC at heights of 0-2 km above cloud base (there is insufficient data for the 3 km level as shown in the figure; therefore, it is not used in the evaluation). The LWC at a height of 2 km above cloud base first reaches a maximum value of 0.7 g m^3 about 9 min after first detection. The LWC at 1 km then peaks at a value of 0.47 g m^{-3} about 2 min later. Finally, the LWC at cloud base peaks at the lowest maximum of 0.35 g m^{-3} about 5 min after the LWC at 2 km reaches its peak. At heights of 4-6 km above cloud base, the LWC was relatively small

(< 0.05 g m^{-3}) as observed in Fig. 1. The minimal LWC at these heights is reasonable because they are located above the 0° C isotherm and the hydrometeors are mostly ice. Also, analysis of vertical structure (not shown) indicates that reflectivity decreases rapidly at these heights, which is consistent with diminishing LWC with height indicated in the results. This pattern was consistent for the other analyzed cases.

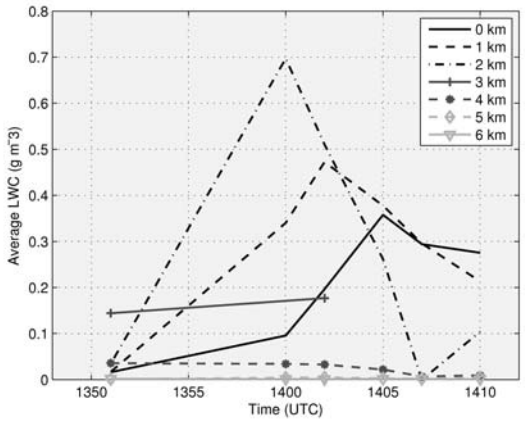

Figure 1. Average radar-derived Liquid Water Content at heights of 0-6 km above cloud base for Cell 1 on 24 July 2006.

Figure 2 shows the average fractional change in the LWC for all the unseeded cases normalized by the maximum LWC for heights 0-4 km above cloud base. As defined in equation (5), positive values indicate an increase in LWC while the negative values indicate a decrease in LWC with increasing time. The change in LWC for heights of 0-2 km above cloud base is positive (but decreasing in relative difference) in the first 18 min after first detection. The LWC decreases slightly between time steps for the period of 18 and 32 min after first detection (AFD) for heights 0-2 km above cloud base. The LWC then increases at heights of 1 and 2 km through 48 min AFD. The changes in LWC for 3-4 km remain positive for the entire lifecycle of the cell. However, there were not many data points at 3 and 4 km; hence, the results may not be representative of the actual variations in LWC at these heights. Note that the large variations after 48 min are an artifact due to the limited number of data points available in the averaging.

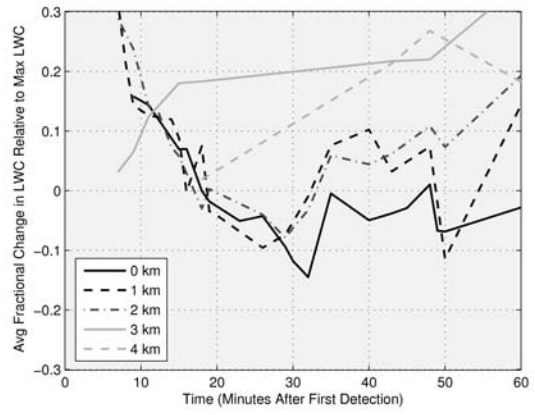

Figure 2. Average fractional change in the radar-derived LWC relative to the maximum radar-derived LWC for all unseeded cases at heights of 0-4 km above cloud base.

b. Seeded Cases

The seeded cases showed some positive results overall. Seven of the eight cases showed an increase in LWC after the initial seeding. The one case that showed a decrease in LWC, which was observed on 24 July 2006, was located along the edge of a larger, more stratiform precipitation area with embedded convection as shown in Fig. 3 (the seeded cell is indicated by the arrow). This cell did not last very long as it combined with the stratiform precipitation and was no longer discernable after several sector scans.

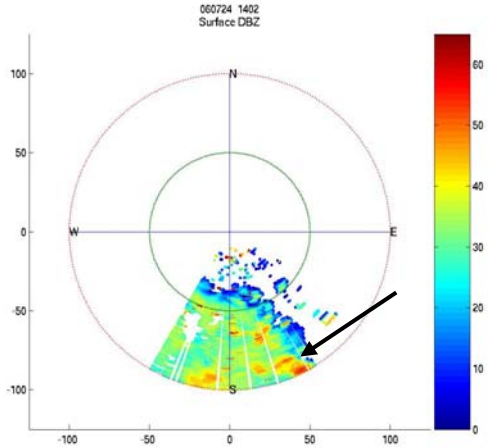

Figure 3. PPI image of reflectivity at 0.5° elevation for the 1402 UTC 24 July 2006 scan. The case in which there was a decrease in LWC after seeding is indicated by the arrow.

The average fractional change in LWC relative to the maximum LWC for the seeded cases can be seen in Fig. 4. The same technique was used to generate the results that were shown for the unseeded cases in Fig. 2. At heights of 1 and 2 km, there was a positive change in LWC from first detection through

30 min. The change was relatively constant until 27 min AFD, at which time the LWC at heights of 1 and 2 km tends to decrease or remain relatively constant for the remaining lifecycle of the cell. At cloud base (e.g., 0 km), there is a steady upward trend in LWC (the variations are likely due to sampling noise and natural variations in the cell) until 40 min AFD. After this time, the LWC decreases throughout the remaining lifecycle of the cell.

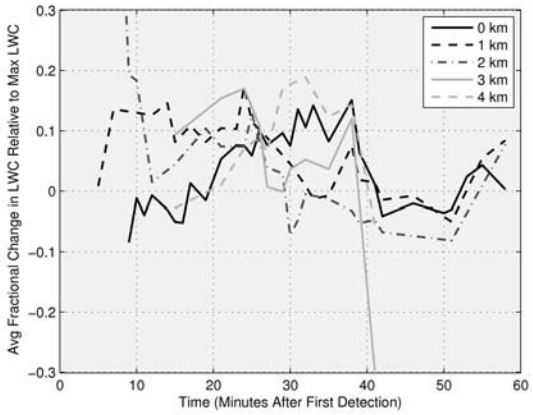

Figure 4. Average fractional change in the radar-derived LWC relative to the maximum radar-derived LWC for all seeded cases for heights of 0-4 km above cloud base.

At heights of 3 and 4 km (as shown in Figs. 2 and 4), there are noticeable differences between the patterns for unseeded and seeded cases. The results should be interpreted carefully as the number of data points at the upper levels was often limited. However, the differences at the upper heights are interesting and worth mentioning. The unseeded cases show smaller fractional changes overall than the seeded cases. The seeded cases on average have longer periods of continuous LWC increases and do not fluctuate between increasing and decreasing as much as the unseeded cases. The main difference occurs between 20 and 30 min when the LWC in unseeded cells was decreasing and the LWC of seeded cells was increasing.

Figure 5 shows the estimated fractional change in LWC relative to the start of the initial flare. The results for heights of 1 and 2 km show an increase in LWC before the initial flare with a larger increase that occurs a few minutes after the initial flare. The results at the 0 km level indicate a decrease in LWC after the initial flare before a large increase in LWC that occurs after 8 min from the initial flare. It is hard to be certain about the physical processes occurring at cloud base. Note that the large variation in LWC at all heights before -10 min is due to the small sample as the cells are in the first detection stage during this time. It is hard to know for sure why the LWC decreased at cloud base just after the initial flare while the upper levels increased in LWC without *in situ* aircraft measurements. However, one hypothesis could be that the seeding material was lifted in the updraft to 1-2 km before precipitation formation occurred. After 8-10 min, the precipitation started falling toward and reached cloud base.

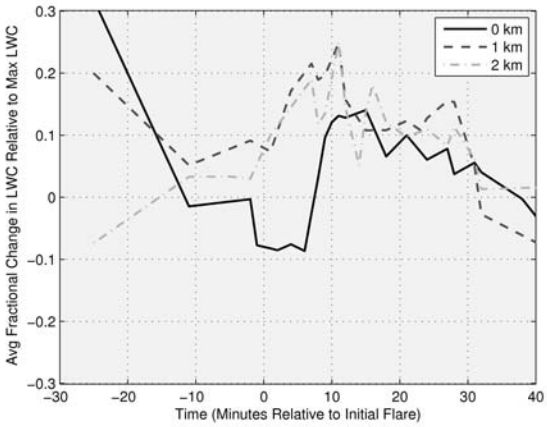

Figure 5. Average fractional change in the radar-derived LWC relative to the maximum radar-derived LWC for all seeded for heights of 0-2 km above cloud base relative to the time of the initial flare.

The maximum liquid water content for both the seeded and unseeded cases at heights of 0 to 5 km above cloud base is summarized in the bar graph shown in Fig. 6. The comparison shows positive results for the seeded cases. The seeded cases have a larger average maximum LWC than the unseeded cases at all heights. The average LWC for seeded cases increases from 0.55 g m^{-3} at cloud base to a maximum of 1.55 g m^{-3} at 3 km above cloud base. The average LWC remains between 0.9 and 1.0 g m^{-3} at heights of 4 and 5 km. In contrast, the average LWC for unseeded cases is nearly constant, centered on 0.4 g m^{-3} to a height of 2 km before decreasing to a minimum of less than 0.1 g m^{-3} at a height of 5 km above cloud base. The seeded cases had a higher average maximum LWC than the unseeded cases by 0.6 $\pm$ 0.4 g m^{-3} or about 66% greater. There is a large standard deviation with the results since there are not a lot of cases, and there is a lot of variability in the range of LWC values. There is definitely a difference between the seeded and unseeded cases, which may or may not be due to seeding. Based on these results,

however, there is evidence that further exploration is needed to confirm if these results are significant.

The time for the cases to reach the maximum LWC for heights of 0-5 km above cloud base for the unseeded and seed cases is shown in Fig. 7. The average time for seeded cases to reach the maximum LWC ranged from 17 min at a height of 5 km to a maximum of 26 min at 3 km above cloud base. In contrast, the seeded cases had a range of 7 min at a height of 5 km and to a maximum of 22 min at a height of 2 km above cloud base. The greatest difference between the seeded and the unseeded cases occurs at 5 km above cloud base with a difference of approximately 9 min. The seeded cases took 4.7 $\pm$ 3.1 min longer to reach the maximum LWC than the unseeded. In summary, the unseeded cases reach the maximum LWC more rapidly AFD than the seeded cases at all heights except for 2 km above cloud base in which the times are close to the same. Again, there is enough evidence that the difference in the seeded and unseeded cases should be explored further.

To summarize, the average radar derived LWC results do show a greater period of increase after first detection by radar for the seeded cases than in the unseeded cases. The unseeded cases also fluctuated a lot more between increasing and decreasing of the LWC. The maximum LWC that is reached by the cells occurs faster in the unseeded cases than in the seeded cases except for the 2 km level above cloud base. The average LWC maximum that occurs for the seeded cases is slightly greater than in the unseeded cases at heights of 0-1 km and by a fairly large amount at heights of 2-5 km. Overall, the LWC has shown some interesting results, indicating that the effects of seeding may be observable by polarimetric radar.

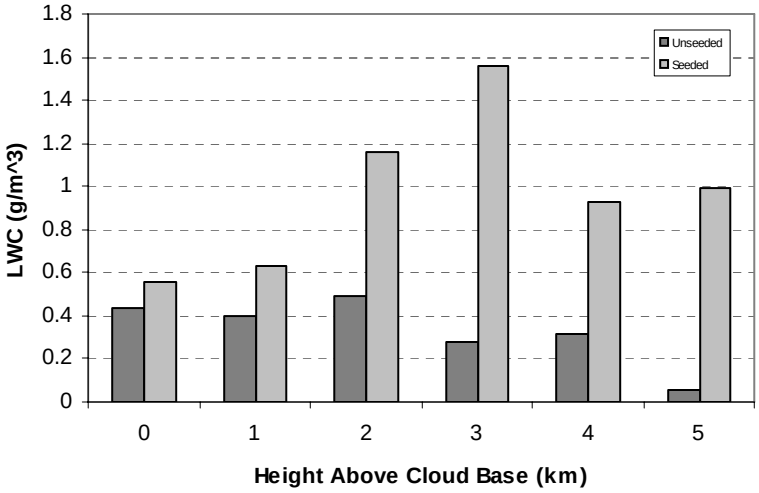

Figure 6. The average maximum radar-derived LWC for heights of 0-5 km above cloud base for the unseeded (dark gray) and seeded (light gray) cases.

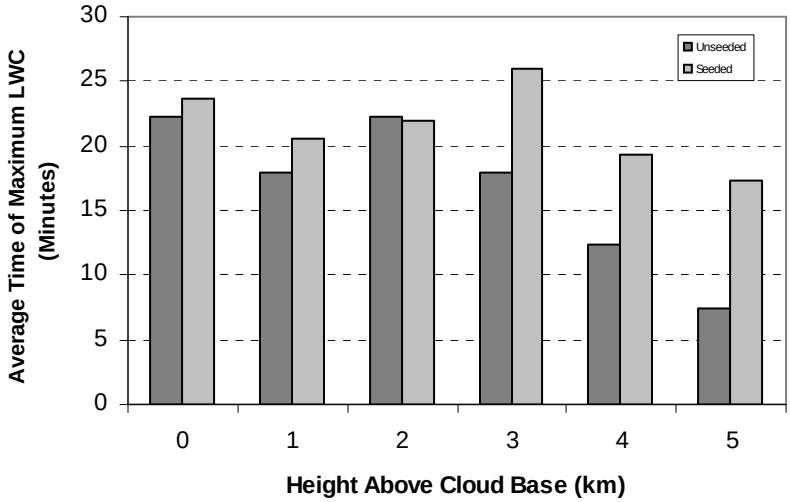

Figure 7. Average time of maximum radar-derived LWC after first detection by radar for unseeded (dark gray) and unseeded (light gray) cases.

II. Differential Reflectivity (ZDR) and Reflectivity

The differential reflectivity analysis produced some interesting results as indicated in Fig. 8. Between 0 and 8 min after initial flare, there is decrease in ZDR at all levels between 0-2 km. The largest decrease occurred at 1 km (as much as 15% relative to the maximum ZDR) followed closely by the decrease at 2 km. The change at cloud base was considerably less with maximum decrease of about 6%. This decrease in differential reflectivity after seeding indicates that the drops are becoming smaller on average in the radar sample volume. After about 8 min, the results show an increase in differential reflectivity at 1 and 2 km, which indicates the raindrops, on average, are increasing in size in the sample volume. After about 15 min, ZDR at 0-2 km levels off and fluctuates about a fairly constant value on average. A possible explanation of this delayed response in differential reflectivity may be due to the time that it takes for the seeding material to be dispersed into the cloud. Shortly after the hygroscopic seeding material is lifted into the cloud by the updraft, water begins condensing on the nuclei. Following this idea, there should be an increase in the number of small raindrops due to seeding. As a result, there could be a lowering of ZDR initially after seeding before the raindrops begin to grow in size; hence becoming more oblate in shape, which would result in a increase in ZDR.

The average fractional change in reflectivity normalized by the maximum reflectivity is shown in Fig. 9 for heights of 0-2 km above cloud base. The change in reflectivity at 1 km above cloud base has an interesting pattern compared to cloud base and at 2 km. At a height of 1 km, there is a positive increase in reflectivity, reaching a peak about 7 min after the initial flare. The change in reflectivity decreases afterwards, and at 11 min after initial flare, the average reflectivity at each time step is lower than the previous time step. The change in reflectivity becomes positive about 26 min after the initial flare. In comparison, the change in reflectivity at cloud base and 2 km is positive before the time of initial flare and remains relatively constant, with the exception of the reflectivity at 2 km which decreases steadily after 17 min from the initial flare, and throughout the remaining analysis period. Analyzing the time period in which there was a large decrease in differential reflectivity, it can be seen that the reflectivity values at 1 and 2 km above cloud base are showing an increase (1 km) or a constant trend (2 km) during that time. Even though the results are indicating that the raindrops are becoming smaller, the increase in reflectivity indicates that there are more raindrops. At a height of 0 km, a slight decrease in reflectivity is observed which is consistent with a slight decrease in differential reflectivity. Since the seeding is below cloud base, the nuclei will begin producing small raindrops, thereby decreasing the reflectivity and differential reflectivity in the sample volume. Then, as these raindrops are lifted into higher levels, they may become larger and more numerous, thereby increasing the reflectivity. However, these raindrops would still have to be smaller than the average raindrops at that level in order for the differential reflectivity to decrease.

In summary, the results from the differential reflectivity analysis indicate a decrease in ZDR after seeding. The reflectivity analysis does indicate a

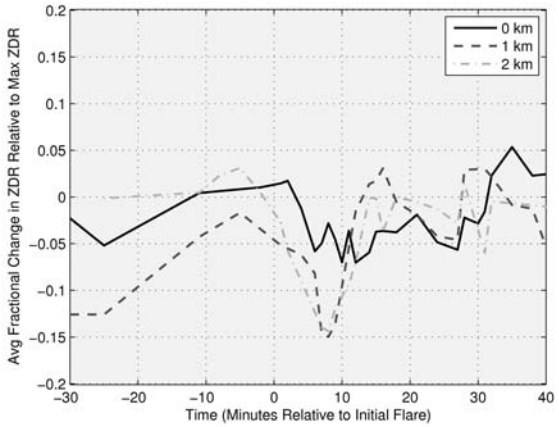

Figure 8. Average fractional change in the ZDR relative to the maximum ZDR above cloud base for all the seeded cases for heights of 0-2 km above cloud base after initial flare.

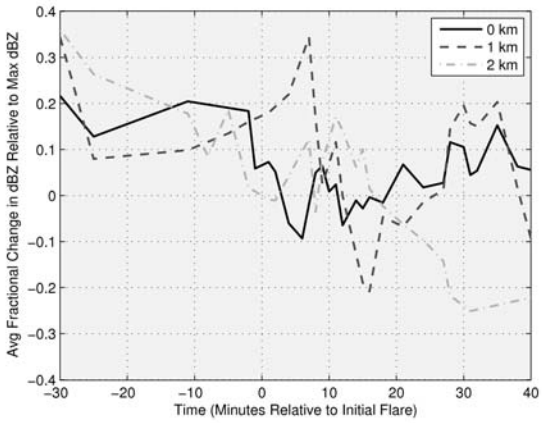

Figure 9. Average fractional change in the reflectivity relative to the maximum reflectivity for heights of 0-2 km above cloud base for the seeded cases after initial flare.

positive to neutral trend above cloud base and slight decrease at cloud base during this same time period. This is in disagreement with the hypothesis that hygroscopic seeding produces larger drops overall. It can be hypothesized why there is a disagreement with current hygroscopic seeding theory. From a radar sampling perspective, the beam spreading and averaging of echo outside the main convective core will result in a contribution in the returned signal from hydrometeors located in these regions. From the results, this would suggest that the raindrops, on average, that are located outside the main updraft (e.g., outside the area of the release of the hygroscopic seeding material) are decreasing in size. If this is occurring, then the seeding effect is overcoming the general trend 7 min after the initial flare.

From a microphysical viewpoint, one can make the argument that the initial augmented droplet spectrum would see a reduction in ZDR due to the activation of many smaller droplets and the formation of smaller raindrops initially, but that the higher reflectivity (e.g., more condensed water) is the initial signature of seeding. Over time, the spectrum broadens as the relatively few droplets created by the larger CCN coalesce (see Roelof et al. (2005) for a plot of the CCN spectrum for the hygroscopic flares) with the more numerous smaller droplets naturally present and those additionally formed by the peak of the flare spectrum.

One issue that has not been addressed is sampling errors. Because of attenuation, Mie scattering, and other propagation effects at C-Band, there could be significant errors in ZDR (and reflectivity). Identification and corrections if necessary will be included in future radar analysis. In any case, these initial results are very interesting. Further exploration of seeding signatures using polarimetric radar observations is clearly needed.

III. Rainfall Rates

The rainfall rate field was averaged over the base scan of 0.5° for each time interval and the time of peak rainfall rate and the total duration of the rain event were calculated. The results of these calculations are shown in Fig. 10. A positive trend for seeded cells is observed for both time of peak rainfall rate and rain duration. Figure 10 indicates that the time it takes to reach the average maximum rain rate is 4.0 $\pm$ 2.8 min longer in the seeded than in the unseeded cases. The duration of the cells was 8.3 $\pm$ 5.8 min longer in the seeded than the unseeded cases. The maximum peak rain rate was 1.5 $\pm$ 1.1 mm h^{-1} greater in the seeded cases, or about 14.8%. This is consistent with other reported results. For example, Yan Yin et al. (2001) also found that hygroscopic seeding should initiate the rain earlier, produce more rain and have a longer duration. In summary, the analysis of seeded cases indicated positive results for the cases analyzed in the study.

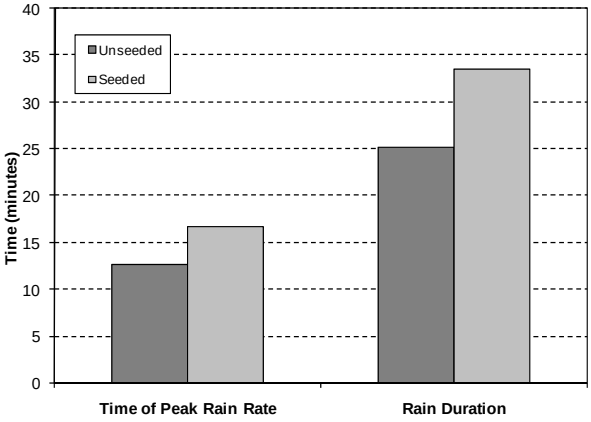

Figure 10. Average time of peak rainfall rate and rainfall duration for the unseeded (dark gray) and seeded (light gray) cases.

.

IV. Hydrometeor Identification

The results from the hydrometeor identification algorithm produced inconclusive, but interesting results. Since the reflectivity is increasing and the differential reflectivity is decreasing, it may give the appearance of hail or graupel as seen in Fig. 11. There was not any hail reported with these cells, but there is an indication of it with the hydrometeor identification program. This was the time during which the seeding was occurring. Comparing the seeded cell to an unseeded cell in Fig. 12, the hydrometeor identification program indicated more hail and graupel in the seeded case, especially in the upper levels. These two cells were taken from the same day, were near the same point in their lifecycles, and hail was not reported for either of them.

A different case did not show hail and graupel at the lower levels until after seeding was complete as seen in Fig 13. The region of hail and graupel in the upper portions of the cell stay close to the same size and shape, but after seeding a column of hail and graupel looks to extend upward from the ground. As with the other cases, there was no hail reported with this cell.

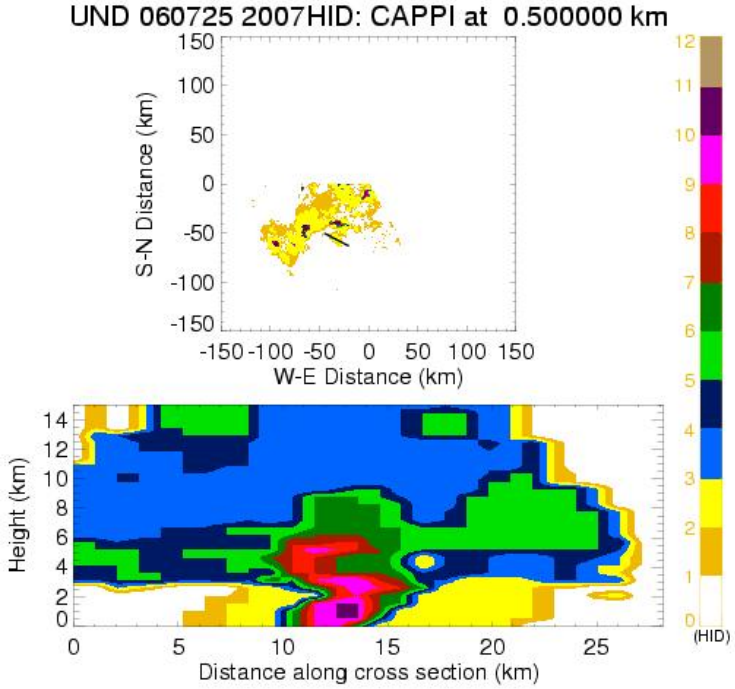

Figure 11. Hydrometeor Identification for 2007 UTC 25 July 2006 (see Table 1 for colorbar definition).

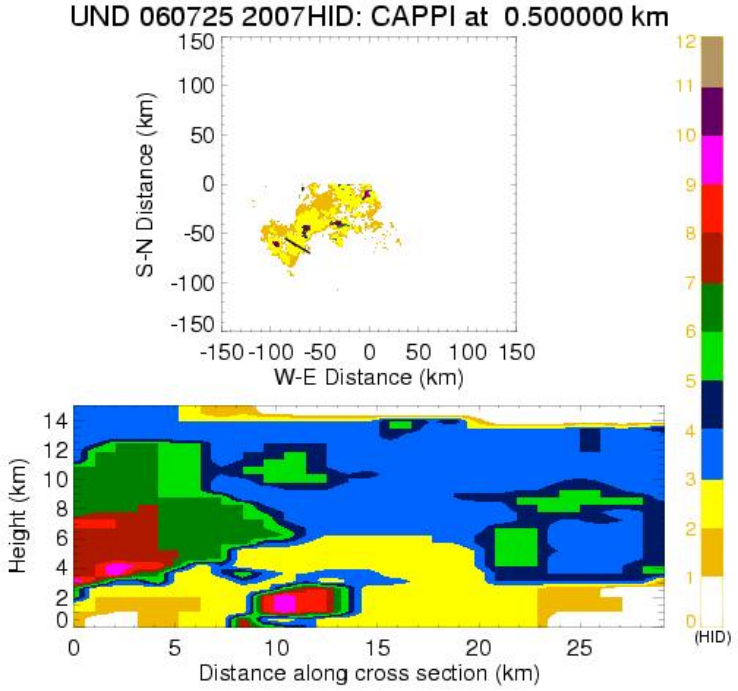

Figure 12. Same as Fig. 11 except for an unseeded case.

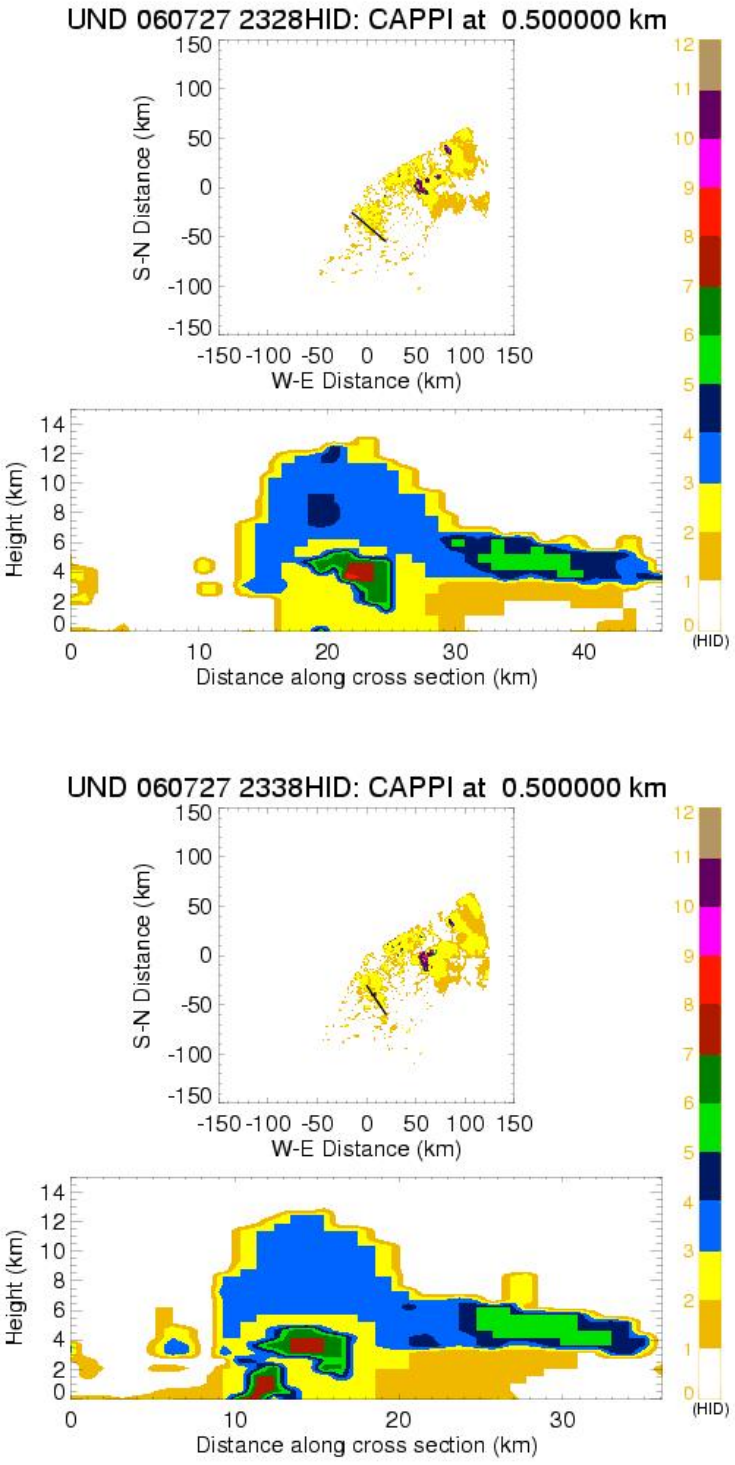

Figure 13. Hydrometeor identification retrieval: Left panel: During seeding at 2328 UTC. Right panel: After seeding was complete at 2338 UTC for the 27 July 2006 case.

The hydrometeor identification program does agree with the trends seen in the reflectivity and ZDR. The reflectivity was increasing and the differential reflectivity was decreasing, indicating that the hydrometeors are able to reflect more power and are becoming more spherical or the orientation is becoming more randomly distributed (e.g., tumbling), which is indicative of graupel and hail, and seen in the hydrometeor identification images.

Uncertainty exists as to the type of hydrometeors in these cases without *in-situ* measurements from aircraft or coincident observations on the ground. Although, it is not possible to confirm that these differences are due to seeding, the observations provide an initial indication of hydrometeor variability within a convective system and should be explored further in future studies. It does appear that the feature in the seeded cell may be from the hygroscopic seeding.

5. Conclusions

POLCAST was an exploratory hygroscopic seeding experiment conducted over parts of eastern North Dakota from 10 July – 5 August 2006. The primary goal of the program was to determine the extent to which hygroscopic seeding signatures may be detected by polarimetric radar observables. From the radar observations, derived fields of liquid water content, rainfall rates, and hydrometeor type were analyzed, and distributions of these fields were compared between seeded and non-seeded convective systems.

It should be noted that the findings of this study are of a preliminary nature. Only eight seeded cases comprise the dataset, far too few to produce any statistically significant results. Selection bias is another issue that must be considered, as the program was not randomized. A number of previous studies have shown that experienced weather modification pilots are very good at determining which clouds have the best chance of producing rain. The next logical step is the design and conduct of a randomized program to more clearly determine the effects of hygroscopic flare seeding on North Dakota convective clouds as viewed by NorthPol.

With that in mind, however, POLCAST did yield some interesting outcomes worthy of additional research. The results from the radar-derived LWC indicate, on average, an increase in LWC after hygroscopic seeding. The one case that did not show an increase in LWC was located along the edge of a larger, more stratiform area of precipitation. The ZDR results indicated that the raindrops are smaller after the initial flare, while the reflectivity increased in the upper-levels. It is difficult to be certain, however, due to the susceptibility of attenuation or other artifacts at C-Band. The rainfall rate analysis also indicated positive results, with an increase in average maximum rainfall rate and rain duration. The hydrometeor identification program produced results in agreement with the ZDR and reflectivity trends. Lowering ZDR and increasing reflectivity would indicate graupel or hail, which is what the hydrometeor identification program was indicating, even though there was no hail reported with either of the cases analyzed. There is considerable uncertainty in hydrometeor identification retrievals without proper verification of the algorithm; this requires surface observations. Though this was a limited and exploratory study, there are indications that polarimetric radar can distinguish the effects of hygroscopic seeding.

6. References

Austin, P. M., 1987: Relation between measured radar reflectivity and surface rainfall. *Mon. Wea. Rev.*, **115**, 1053-1070.

Bringi, V. N and V. Chandrasekar, 2001: *Polarimetric Doppler Weather Radar*. Cambridge University Press, 629 pp.

Bringi, V. N., K. Knupp, A. Detwiler, L. Liu, I. J. Caylor, and R. A. Black, 1997: Evolution of a Florida thunderstorm during the convection and precipitation/electrification experiment: The case of 9 August 1991. *Mon. Wea. Rev.*, **125**, 2131-2160.

Bruintjes, R. T., V. Salazar, G. L. Kok, D. W. Breed, and J. Gunkelman, 2005: Design and testing of a hygroscopic cloud seeding flare test facility. Submitted to *J. Wea. Modification*.

Carey, L., and S. A. Rutledge, D. A. Ahijevych, and T. D. Keenan, 2000: Correcting propagation effects in C-band polarimetric radar observations of tropical convection using differential propagation phase. *J. Appl. Meteor.,* **39,** 1405–1433.

Hu, Z., R. T. Bruintjes, and E. A. Betterton, 1998: Sensitivity of cloud droplet growth to collision and coalescence efficiencies in a parcel model. *J. Atmos. Sci.*, **55**, 2502-2515.

Hudak, D. R. and R. List, 1988: Precipitation development in natural and seeded cumulus clouds in southern Africa. *J. Appl. Meteor.*, **27**, 734-756.

Kennedy, P. C., S. A. Rutledge, W. A. Peterson, and V. N. Bringi, 2001: Polarimetric radar observations of hail formation. *J. Appl. Meteor.,* **40**, 1347-1366

Marshall, J. S. and W. M. K. Palmer, 1948: The distribution of raindrops with size. *J. Meteor.*, **5**, 165-166.

May, P. T. and T. D. Keenan, 2005: Evaluation of microphysical retrievals from polarimetric radar with wind profiler data. *J. Appl. Meteor.*, **44**, 827-838.

Liu, H., and V. Chandrasekar, 2000: Classification of hydrometeors based on polarimetric radar measurements: Development of a fuzzy logic and neurofuzzy systems, and in situ verification. *J. Atmos.Oceanic Technol.,* **17**, 140–164.

Straka, J. M., D. S. Zrnic, and A. V. Ryzhkov, 2000: Bulk hydrometeor classification and quantification using polarimetric radar data: Synthesis of relations. *J. Appl. Meteor.*, **39**, 1341-1372.

Tzivion, S., T. Reisen, and Z. Levin, 1993: Numerical simulation of hygroscopic seeding in a convective cloud. *J. Appl. Meteor.*, **33**, 252-267.

Yin, Y., Z. Levin, T. Reisen, and S. Tzivion, 2001: On the response of radar-derived properties to hygroscopic flare seeding. *J. Appl. Meteor.*, **40**, 1654-1661.